

**Bosonic excitations and electron pairing in an electron-doped cuprate superconductor**M. C. Wang,<sup>1</sup> H. S. Yu,<sup>2,3</sup> J. Xiong,<sup>4</sup> Y.-F. Yang,<sup>2,3</sup> S. N. Luo,<sup>1</sup> K. Jin,<sup>2,3,\*</sup> and J. Qi<sup>1,4,†</sup><sup>1</sup>*The Peac Institute of Multiscale Sciences, Chengdu 610031, China*<sup>2</sup>*Beijing National Laboratory for Condensed Matter Physics, Institute of Physics, Chinese Academy of Sciences, Beijing 100190, China*<sup>3</sup>*Collaborative Innovation Center of Quantum Matter, Beijing 100190, China*<sup>4</sup>*State Key Laboratory of Electronic Thin Films and Integrated Devices, University of Electronic Science and Technology of China, Chengdu 610054, China*

(Received 24 January 2018; published 27 April 2018)

By applying ultrafast optical spectroscopy to electron-doped  $\text{La}_{1.9}\text{Ce}_{0.1}\text{CuO}_{4\pm\delta}$ , we discern a bosonic mode of electronic origin and provide the evolution of its coupling with the charge carriers as a function of temperature. Our results show that it has the strongest coupling strength near  $T_c$  and can fully account for the superconducting pairing. This mode can be associated with the two-dimensional antiferromagnetic spin correlations emerging below a critical temperature  $T^\dagger$  larger than  $T_c$ . Our work may help to establish a quantitative relation between bosonic excitations and superconducting pairing in electron-doped cuprates.

DOI: [10.1103/PhysRevB.97.155157](https://doi.org/10.1103/PhysRevB.97.155157)**I. INTRODUCTION**

In unconventional superconductors, such as high- $T_c$  cuprates, it has been a longstanding challenge to reveal the effective interaction of charge carriers (fermionic quasiparticles) with phonons or other bosonic excitations of electronic origin [1–3]. In particular, huge efforts have been made to unravel the electronic excitations likely giving rise to the superconducting (SC) pairing, such as charge, spin, and orbital fluctuations [2–8]. However, an unambiguous solution to the pairing issue remains obscure because it is extremely difficult to quantitatively identify the most relevant bosonic excitations and their related interactions near  $T_c$  due to various types of excitations entangled in the energy domain [9–12].

Ultrafast optical spectroscopy provides a unique opportunity to directly probe the related interactions in the time domain [13]. Its capability of distinguishing between phonons and other bosons of electronic origin has also been investigated both experimentally and theoretically [14,15]. Under nonequilibrium conditions, these bosonic modes display distinct relaxation dynamics because of their different couplings to the charge carriers and may thereby be potentially disentangled. This technique has been extensively utilized in studying the SC gap, pseudogap, and competing orders on high- $T_c$  superconductors [16–21], but its application on unveiling the entangled bosonic excitations and their temperature evolution remains elusive [13,22,23].

In this work, by measuring the transient optical reflectivity change  $\Delta R(t)/R$  as a function of temperature, we unravel different bosonic modes and investigate their peculiar relaxation dynamics in the electron-doped cuprates  $\text{La}_{2-x}\text{Ce}_x\text{CuO}_{4\pm\delta}$  (LCCO). Unlike their hole-doped counterparts, where superconductivity is often intertwined with anomalous pseudogap, the electron-doped cuprates are relatively simple and believed

to exhibit prominent antiferromagnetic (AFM) spin fluctuations (or correlations) [24,25]. In fact, our LCCO samples are optimally doped with a Ce concentration of  $x = 0.1$ , which sits near the AFM border in the temperature-doping ( $T$ - $x$ ) phase diagram [26]. The temperature-dependent results enable us to identify with confidence a bosonic mode of electronic origin that is closely related to the two-dimensional (2D) AFM spin fluctuations. We discover an enormous enhancement of its interaction with fermionic quasiparticles as temperature decreases from high temperatures down to  $T_c$ . We demonstrate that this bosonic mode is of critical importance for the electron pairing and can fully account for the SC  $T_c$ .

**II. EXPERIMENT**

Figure 1(a) shows the typical ultrafast optical pump-probe spectroscopy setup [27,28]. The time-resolved transient reflectivity change  $\Delta R/R$  was measured using a Ti:sapphire oscillator lasing at the center wavelength of 800 nm ( $\sim 1.55$  eV). It has a repetition rate of 80 MHz and a pulse duration of  $\sim 35$  fs. The pump beam, with a typical fluence of  $\sim 0.3$   $\mu\text{J}/\text{cm}^2$ , directs along the normal incidence and is kept  $p$  polarized. The probe beam, with a typical fluence of  $\sim 0.03$   $\mu\text{J}/\text{cm}^2$ , is incident at a  $\sim 10^\circ$  angle to the sample normal and is kept  $s$  polarized. In order to evaluate the cumulative heating effect, we also performed the fluence-dependent experiments using a similar setup with a Ti:sapphire laser system with a low repetition rate of 5.1 MHz and a pulse duration of 60 fs (see Appendix A). The  $c$ -axis-oriented LCCO ( $x = 0.1$ ) thin films with a thickness of 100 nm were deposited on the (00 $l$ )-oriented SrTiO<sub>3</sub> substrates by a pulsed laser deposition system. Details on the sample preparation and characterization are given in the Supplemental Material [29].

**III. RESULTS AND DISCUSSION**

Figure 1(b) displays the obtained  $\Delta R(t)/R$  as a function of temperature within  $\sim 10$  ps in four optimal-doped

\*kuijin@iphy.ac.cn

†jbqi@uestc.edu.cn

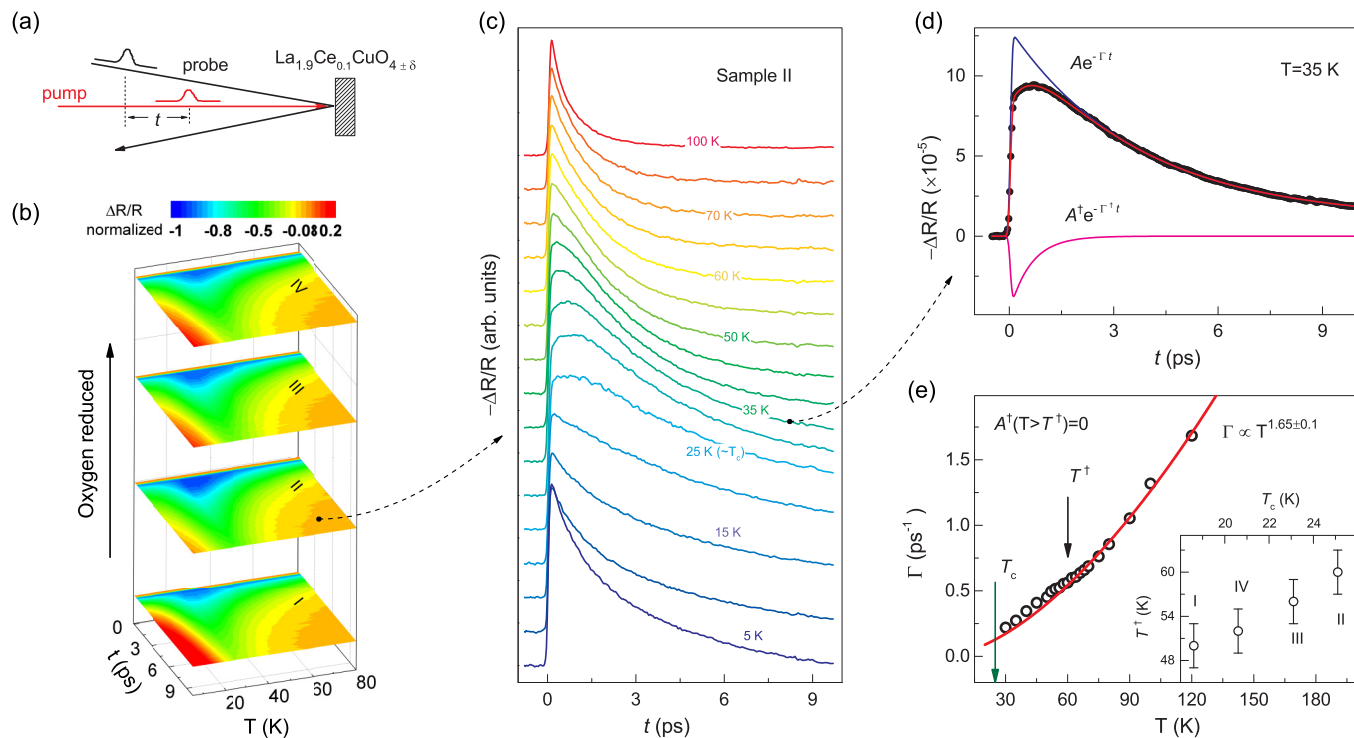


FIG. 1. Temperature-dependent  $\Delta R(t)/R$  in optimally doped  $\text{La}_{1.9}\text{Ce}_{0.1}\text{CuO}_{4\pm\delta}$ . (a) Schematic of optical pump-probe experimental setup. (b)  $\Delta R(t)/R$  as a function of temperature in four different samples, I, II, III, and IV, with different oxygen concentration  $\delta$ . (c) Detailed plot of  $\Delta R(t)/R$  measured in sample II. (d) A typical fitting of  $\Delta R(t)/R$  at 35 K using two exponential decays shown by the red line. Two decay components are indicated by the blue ( $Ae^{-\Gamma t}$ ) and magenta ( $A^\dagger e^{-\Gamma^\dagger t}$ ) lines. (e) The  $\Gamma$  values at  $T > T_c$  follow well a power law:  $\Gamma \propto T^{1.65 \pm 0.1}$ . The black and green arrows indicate the positions of  $T^\dagger$  and  $T_c$ , respectively. Inset:  $T_c$  increases monotonically with  $T^\dagger$  for the investigated samples.

$\text{La}_{1.9}\text{Ce}_{0.1}\text{CuO}_{4\pm\delta}$  with different  $\delta$ . The signals from different photoexcitation spots in all samples are very consistent but behave distinctively in separate temperature regimes. Figure 1(c) plots  $\Delta R(t)/R$  measured in sample II ( $T_c = 25.1$  K). The relaxation seems to take simple exponential decay at both high and low temperatures. However, a peculiar and relatively slow rising process following the initial instantaneous uprising is observed at intermediate temperatures between  $\sim 25$  and  $\sim 60$  K as manifested by the bumplike behavior after  $\sim 100$  fs. This type of signal corresponds to the dark blue region in Fig. 1(b) and seems to be quite common in cuprates [19–21]. Due to similarities between the four samples, all detailed analyses below are for data taken from sample II except where noted.

We focus mainly on the experimental data for  $T > T_c$ , measured with low pump fluence, so that we can ignore the complexity of interpreting the quasiparticle dynamics in the SC state [30]. As seen in Fig. 1(d),  $\Delta R(t)/R$  with the bumplike feature can be well fitted using a function of the form  $\Delta R(t)/R = Ae^{-\Gamma t} + A^\dagger e^{-\Gamma^\dagger t} + D$ , where  $A$  (or  $A^\dagger$ ) and  $\Gamma$  (or  $\Gamma^\dagger$ ) are the amplitude and decay rate, respectively.  $D$  is a  $t$ -independent offset. Specifically,  $A^\dagger = 0$  for  $T > T^\dagger$  ( $T^\dagger \simeq 60$  K). The emergence of the nonzero  $A^\dagger$  component indicates the onset of a new scattering channel between quasiparticles and bosons around  $T^\dagger$ . Since this change occurs instantaneously after photoexcitation, we expect that it is caused by bosonic excitations that are strongly coupled with the nonequilibrium quasiparticles in the initial relaxation

dynamics. Figure 1(e) plots the decay rate  $\Gamma$  for  $T > T_c$ , where we find the data nearly follow a power law:  $\Gamma \propto T^\alpha$  ( $\alpha \simeq 1.65 \pm 0.1$ ). In fact, below  $\sim 0.3 \mu\text{J}/\text{cm}^2$ ,  $\Gamma$  is nearly fluence independent for  $T > T_c$  (see Appendix A). Therefore, low pump fluence is crucial as it helps yield fluence-independent parameters and enables us to extract accurate physical information using the fitting model described below. At high pump fluences,  $\Gamma$  below  $T^\dagger$  will obviously deviate from this power law (see Ref. [21] and Appendix A). Similar scaling has also been observed in the  $T$ -dependent resistivity [24,31], suggesting an intimate connection between the resistivity scaling and the coupling to the bosonic excitations. In addition, we surprisingly notice that  $T_c$  increases with  $T^\dagger$  for the investigated samples, as seen in the inset of Fig. 1(e). Such a result suggests that the bosonic excitations contributing to the new scatterings emerging below  $T^\dagger$  are closely related to the SC property.

In order to reveal the mechanisms behind our above observations, one common theoretical approach is the effective-temperature model [13]. In the frame of this model, one can understand the temporal evolution of the nonequilibrium state as the energy exchange among the electron and boson reservoirs via the electron-boson and boson-boson scattering processes. However, this model generally can describe well only the case of Fermi-liquid-like systems [13] where the photoexcited hot electrons are quickly quasithermalized via electron-electron ( $e$ - $e$ ) scatterings ahead of the dominant electron-boson interactions. Therefore, it is not appropriate to directly apply the effective-temperature model to a

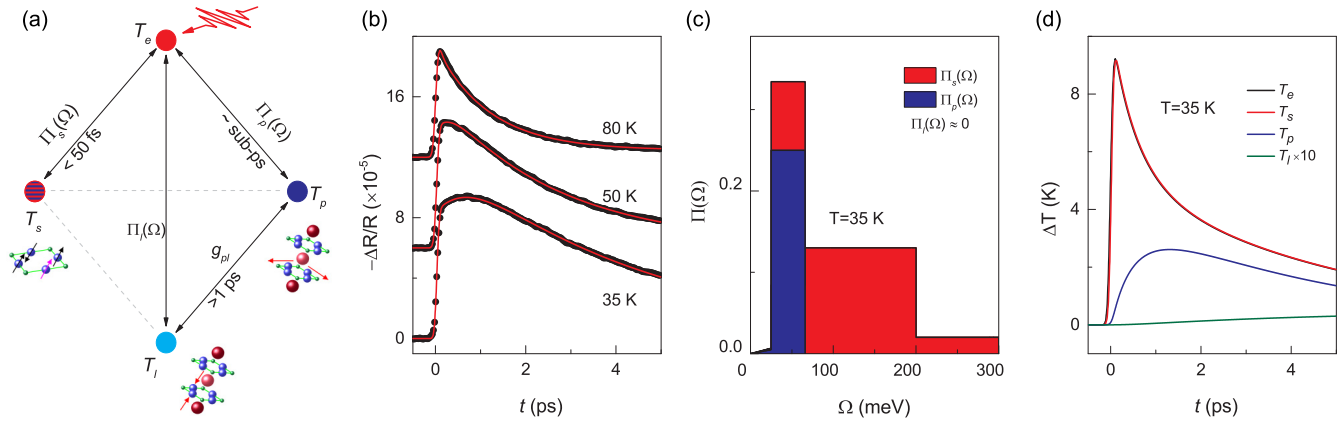


FIG. 2. Typical fitting via the effective-temperature model. (a) Energy relaxations between electrons ( $T_e$ ), bosons with electronic origin ( $T_s$ ), hot phonons ( $T_p$ ), and the rest of the lattice ( $T_l$ ) are described by the effective-temperature model (Appendix B). The time evolutions of  $T_e$  and  $T_j$  ( $j = s, p, l$ ) are determined by the bosonic spectra function  $\Pi_j(\Omega)$  and the anharmonic phonon decay  $g_{pl}$ . The thermalization timescales are given by the fitted  $T_e(t)$  and  $T_j(t)$ . (b) Fitting results at several typical temperatures. (c) The bosonic function  $\Pi(\Omega)$  obtained by fitting  $\Delta R/R$  at 35 K. The red and blue areas represent  $\Pi_s(\Omega)$  and  $\Pi_p(\Omega)$  associated with the electronic and phononic excitations, respectively. (d) The corresponding  $T_e(t)$  and  $T_j(t)$  at 35 K, characterizing the electrons, bosons with electronic origin, hot phonons, and the rest of the lattice.

photoexcited strongly correlated system in the whole time domain [32]. Instead, one should consider the nonthermal behavior of hot electrons in a more comprehensive model (see Ref. [33] and Appendix B). In addition, in cuprate superconductors under the SC and pseudogap states,  $\Delta R/R$  might directly arise from the spectral weight redistributions due to modifications of these states by the optical pump pulses. Under such conditions, it is not straightforward or very difficult to investigate the electron-boson interactions using the effective-temperature model.

Nevertheless, in the complex hole-doped cuprate  $\text{Bi}_2\text{Sr}_2\text{CaCu}_2\text{O}_{8+x}$  ( $\text{Bi2212}$ ) system, at high temperatures without pseudogap and SC states a quasithermal behavior was observed instantaneously after photoexcitation [14,32,34], and the  $e$ - $e$  scattering time was believed to be less than  $\sim 10$  fs [32]. In addition, the rising time ( $\sim 45$  fs) of  $\Delta R/R$  immediately following the photoexcitation derived from our experimental data is almost equivalent to the optical pulse duration. Such observation suggests an ultrafast  $e$ - $e$  scattering time existing in the LCCO samples because a strong indication of a long  $e$ - $e$  scattering process is that the rising time is much larger than the pulse duration [35]. Therefore, these results imply that at high temperatures, e.g.,  $T > T_C$ , the effective-temperature model might still be applicable when discussing the dynamics in the electron-doped LCCO.

Figure 2(a) illustrates the energy exchanges and relaxation between four reservoirs in the frame of the effective-temperature model: one for the charge carriers and three for the bosonic excitations. Each reservoir is characterized by an effective temperature  $T_e$  or  $T_j$  ( $j = s, p, l$ ). The subscript  $e$  denotes the charge carriers. The bosonic excitations are classified by their electronic origin such as spin fluctuations ( $s$ ) or phononic origin, including hot phonons ( $p$ ) and the rest of lattice excitations ( $l$ ). The time evolution of the effective temperatures is quantitatively connected to the interactions between charge carriers and bosonic modes. The interaction associated with each mode can be fully accounted for by its linear contribution  $\Pi_j(\Omega)$  to the total bosonic spectral function

$\Pi(\Omega)$  [13,14]. Conventionally,  $\Pi_s(\Omega)$  and  $\Pi_{p,l}(\Omega)$  are also expressed as  $I^2\chi(\Omega)$  and  $[\alpha^2 F(\Omega)]_{p,l}$ . In principle,  $T_e(t)$ ,  $T_j(t)$ , and  $\Pi_j(\Omega)$ , which decide the electronic self-energy  $\Sigma(t, \Omega)$ , can be derived from the time-dependent optical conductivity  $\sigma(t, \omega)$  or reflectivity  $R(t, \omega)$  using the extended Drude model [14,34]. Such a relationship provides us with the possibility to disentangle the electronic and phononic excitations and quantitatively elucidate the temperature evolution of their interactions with the fermionic quasiparticles that leads to the electron pairing at  $T_c$ .

However, different from previous work done at room temperature [14], we find that during quasiparticle thermalization it is necessary to include the additional coupling term  $g_{pl}$  describing the anharmonic decay to explain our  $T$ -dependent experiments in the low-temperature regime (see Appendix B). Therefore, hot phonons are an indispensable and dominant scattering medium for the excited quasiparticles to equilibrate with the lattice. In fact, incorporating  $g_{pl}$  eventually leads to a negligible  $\Pi_l(\Omega)$  ( $\simeq 0$ ).

Figure 2(b) shows the fit to experimental data using the effective-temperature model (see Appendix B). Excellent agreement is obtained for all investigated temperatures. In fact, the number of free fitting parameters is even less than that in the simple two-exponential decay equation frequently used for interpreting the time-resolved data. Details on the fitting procedure are provided in the Supplemental Material [29]. During the fitting, the electron-phonon couplings are assumed to be independent of temperature [34,36]. As an example, the total bosonic spectra  $\Pi(\Omega)$  at 35 K and the corresponding  $\Pi_s(\Omega)$  and  $\Pi_p(\Omega)$  [ $\Pi_l(\Omega) \simeq 0$ ] are illustrated using a histogramlike function in Fig. 2(c) [13,14]. In fact, the final fitting results are quite robust against the detailed shape of  $\Pi(\Omega)$  [14]. A crucial result yielded by our fitting is the specific heat associated with  $\Pi_s(\Omega)$ :  $C_s < 0.018C_e$ , as seen in Fig. 3(a). Although we have already pointed out that the  $e$ - $e$  scattering ends rapidly in LCCO, one might still question whether such small  $C_s$  can be contributed by the nonthermalized electrons. Indeed, under the premise of

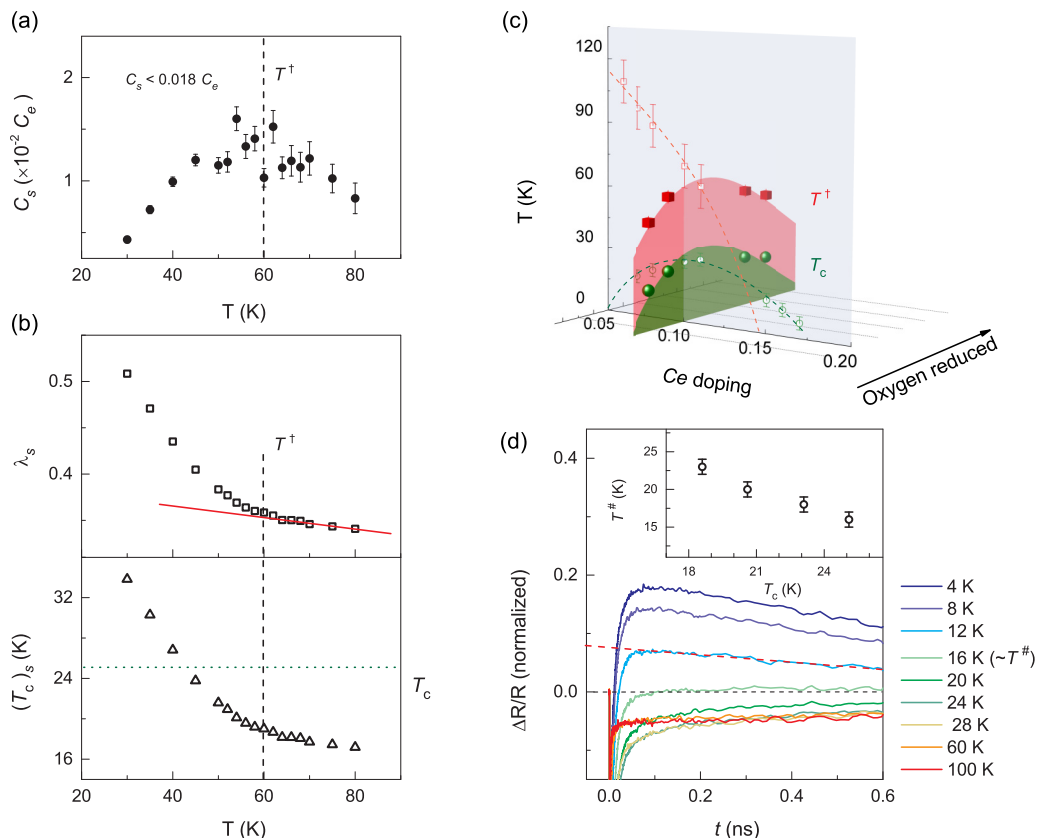


FIG. 3. Temperature-dependent fitting results and the long-relaxation processes in  $\Delta R(t)/R$ . (a) The specific heat  $C_s$  as a function of temperature.  $C_s$  reaches a maximum around  $T^\dagger$ , indicated by the dashed line. (b) The electron-boson coupling constant  $\lambda_s$  as a function of temperature (black open squares). The red solid line indicates the experimental data below the critical temperature  $T^\dagger$  strongly increase with decreasing temperature. The estimated maximum SC transition temperature  $(T_c)_s$  is shown by the black open triangles. The green dotted line indicates  $T_c$  ( $=25.1$  K). The black dashed line shows the position of  $T^\dagger$ . (c)  $T$ - $x$  and  $T$ - $\delta$  phase diagram for LCCO. In the  $T$ - $x$  phase diagram, the green dashed line with open circles represents the SC boundary, while the red dashed line with open squares represents the AFM boundary estimated by the in-plane angular magnetoresistance measurements [24,38]. In the  $T$ - $\delta$  phase diagram, the green area is the SC dome, while the red area, evaluated from this work, represents the 2D AFM spin-fluctuation regime. (d)  $\Delta R(t)/R$  as a function of temperature on a long timescale for sample II. The red dashed line represents the long-relaxation component extending into the nanosecond regime.  $T^\#$  is the critical temperature where the amplitude of the long-relaxation component flips sign.  $T^\#$  as a function of  $T_c$  is shown in the inset.

reasonable fit,  $C_s$  remains almost unchanged even in the frame of the extended effective-temperature model including the nonthermal effect (see Appendix B). Thus, such a small  $C_s$  evidently shows that the bosonic excitations associated with  $\Pi_s(\Omega)$  have an electronic origin, which is further confirmed by the temperature-dependent measurements of  $C_s$  below. This finding is also very consistent with the fact that  $T_e$  and  $T_s$  get instantaneously thermalized, in contrast to the slow rising time of  $T_p$  (subpicosecond) and  $T_l$  ( $>1$  ps) in Fig. 2(d). Although  $\Pi_s(\Omega)$  is distributed over the whole energy domain investigated, its contribution within  $\sim 65$  meV (the upper limit of phonon energy [21,37]), where different types of bosons are entangled, is significant at low temperatures, e.g.,  $\Pi_s/\Pi_p \simeq 0.4$  for  $\Omega \lesssim 65$  meV at 30 K.

Furthermore, our experiments show that  $\Pi_s(\Omega)$  strongly depends on the temperature. Specifically, the strength of  $\Pi_s(\Omega \lesssim 65$  meV), represented by the red area below 65 meV in Fig. 2(c), increases significantly as  $T$  approaches  $T_c$  (see the Supplemental Material [29]). This variation can be best revealed by investigating the temperature-dependent

electron-boson coupling constant:  $\lambda_s = 2 \int \Pi_s(\Omega)/\Omega d\Omega$ . As shown in Fig. 3(b), we clearly observe a pronounced enhancement of  $\lambda_s$  below  $T^\dagger$  ( $\sim 60$  K), corresponding to the strong increase in  $\Pi_s(\Omega \lesssim 65$  meV). Remarkably, there is a peak around  $T^\dagger$  in the specific heat  $C_s$  ( $<0.018 C_e$ ). Nonthermal electrons can hardly contribute to such abnormal  $T$ -dependent behavior. Instead, these results strongly indicate the emergence of electronic excitations with a sufficiently long correlation length below  $T^\dagger$ . Indeed,  $T^\dagger$  is found to have the same temperature scale reported previously, below which the in-plane twofold anisotropic magnetoresistance appears and the 2D AFM correlations are proposed to emerge [24,38]. Therefore, the detected bosonic mode of electronic origin should be closely related to the 2D AFM spin fluctuations. The above observations are in accordance with the remarkable change in experimental  $\Delta R(t)/R$  and also explain the appearance of the  $A^\dagger$  component in  $\Delta R/R$ , which is initially expected to arise from the onset of the new scattering channel.

Assuming that each  $\Pi_j(\Omega)$  ( $j = s, p$ ) entirely contributes to the electron pairing, we are able to estimate

the maximum SC transition temperature  $(T_c)_j$  associated with  $\lambda_j$  via the extended McMillan formula [29,39,40]:  $T_c = 0.83\Omega_j \exp[-1.04(1 + \lambda_j)/\lambda_j]$ , where  $\ln\Omega_j = 2/\lambda_j \int_0^\infty \Pi_j(\Omega) \ln\Omega/\Omega d\Omega$ . The electron-phonon coupling  $\lambda_p$  is found to be  $\sim 0.47$  and agrees well with previous findings in cuprates [13,37]. It correspondingly yields a maximum critical temperature  $(T_c)_p$  of  $\sim 15$  K, which is far below  $T_c (= 25.1$  K). This implies that phonons alone cannot be the key pairing glue. By contrast, the bosonic mode of electronic origin becomes stronger with decreasing temperature. The  $\lambda_s$  at 30 K, as seen in Fig. 3(b), can already yield a maximum  $(T_c)_s$  of 34 K, which is well above the SC transition temperature. This presents direct evidence that the AFM spin fluctuations can fully account for the electron pairing in LCCO. Given the increasing rate of  $\lambda_s$  below  $T^\dagger$  is nearly the same for the investigated samples,  $T_c$  is expected to increase monotonically with  $T^\dagger$  and agree well with the observation in the inset of Fig. 1(e). Extracting  $T^\dagger$  from different optimally doped samples ( $x = 0.1$ ) gives us a new temperature-oxygen concentration ( $T$ - $\delta$ ) phase diagram on top of the previous  $T$ - $x$  phase diagram. The expected SC dome and the 2D AFM spin-fluctuation regime are shown by the green and red regions in Fig. 3(c), respectively. Based on the above analysis, this phase diagram provides evidence that stronger 2D AFM spin fluctuations will give rise to higher  $T_c$  [41].

Nonzero  $\Pi_s(\Omega)$  persists to high temperatures above  $T^\dagger$ , where it is dominantly distributed above  $\sim 65$  meV. The obtained coupling  $\lambda_s$  gradually decreases with increasing temperature. For  $T > T^\dagger$ , the estimated maximum  $(T_c)_s$  becomes comparable to or even smaller than  $(T_c)_p$ . Thus, experiments limited to high temperatures may fail to catch the decisive temperature evolution of bosonic excitations and cannot tell which bosons are truly responsible for the high  $T_c$  in LCCO. At this stage, we cannot clarify the exact origin of the electronic excitations above  $T^\dagger$ . Nevertheless, they may act as an important scattering medium for the  $T^{1.6}$  scaling of the resistivity by quantum criticality at the edge of the superconductivity dome [24,31].

An interesting phenomenon is observed when we turn to the long-relaxation process in the nanosecond regime. In this regime, the relaxation for metalliclike systems is often attributed to the low-energy excitations. As shown in Fig. 3(d), the amplitude of such long-relaxation dynamics changes sign from negative to positive with decreasing temperature. Specifically, it has a negative amplitude at high temperatures, e.g., 100 K, where the long relaxation with the nanosecond timescale should be attributed mainly to the thermal diffusion processes or the dissipation of low-energy acoustic phonons. As the temperature gradually decreases, there appears to be a hidden positive long-decay component which competes with the negative one, shifts the overall long-relaxation signal towards zero at a certain temperature  $T^\#$ , and causes a positive amplitude in the nanosecond regime at lower temperatures, indicated by the red dashed line in Fig. 3(d). We investigated  $T^\#$  in a set of various oxygen-tuned samples and found that  $T^\#$  can be either above or below  $T_c$ . However, more surprisingly, an anticorrelation relation exists between  $T^\#$  and  $T_c$ , as seen in the inset of Fig. 3(d). These phenomena suggest a competing order associated with  $T^\#$  that can coexist with the superconductivity. A natural candidate of such a competing

order is the three-dimensional antiferromagnetism [42]. We note that  $T^\#$  indicates only the existence of the competing order and cannot reveal the exact temperature where it starts to appear. In addition, although below  $\sim 0.3 \mu\text{J}/\text{cm}^2$  the absolute value of  $T^\#$  can change slightly as the pump fluence varies [21], the anticorrelation behavior between  $T^\#$  and  $T_c$  will not change.

#### IV. CONCLUSION

Our results provide quantitative and unambiguous evidence for the electron-doped cuprates known so far that bosons with electronic origin, i.e., 2D AFM spin fluctuations, are the imperative glue for the SC pairing, although we cannot exclude the possibility that other electronic excitations and phonons could also participate in the electron pairing process. Our work demonstrates that ultrafast optical spectroscopy in the temperature domain not only can extract the strongest coupling associated with the electronic excitations near  $T_c$  but also is capable of elucidating the origin of these excitations via their temperature dependence. Therefore, this investigation forges a path for systematically exploring interactions between charge carriers and bosons with both electronic and phononic origins in cuprates and other correlated materials.

#### ACKNOWLEDGMENTS

We thank M. K. Liu for helpful discussions. We acknowledge the support of the Science Challenge Project of China (TZ2016004), the National Key Basic Research Program of China (Grant No. 2015CB921000), the National Natural Science Foundation of China (Grant No. 11474338), and the Beijing Municipal Science and Technology Project (Z161100002116011).

#### APPENDIX A: CUMULATIVE HEATING EFFECT

At low temperatures, possible non-negligible accumulated heating on samples may hinder our attempt to reveal the physics behind using laser systems with a high repetition rate. Therefore, in order to evaluate such an effect, we performed similar experiments using another Ti:sapphire laser system with a lower repetition rate of 5.1 MHz and a pulse duration of  $\sim 60$  fs.

First of all, we note that in this work our main focus is on the experimental data at temperatures above  $T_c$ , i.e.,  $T \gtrsim 30$  K. In the high-temperature regime (normal state), the continuous heating effect is greatly minimized. Second, Fig. 4 illustrates the typical results taken at 35 K for sample I using a 5.1-MHz laser system. For excitation fluences below  $\sim 0.6 \mu\text{J}/\text{cm}^2$ , the normalized  $\Delta R/R$  data follow almost the same time-dependent behavior, or  $\Gamma$  defined in Fig. 1 is nearly fluence independent. For comparison, Fig. 4 also shows the normalized  $\Delta R/R$  measured with a fluence of  $\sim 0.6 \mu\text{J}/\text{cm}^2$  using the 80-MHz laser system. It can be seen that the signal nearly overlaps with those measured below  $\sim 0.6 \mu\text{J}/\text{cm}^2$  using the 5.1-MHz system. These observations imply that for  $T \gtrsim 30$  K the cumulative heating effect is minimized or can be neglected for fluences below  $\sim 0.6 \mu\text{J}/\text{cm}^2$ . The low pump fluence of  $\sim 0.3 \mu\text{J}/\text{cm}^2$  used in our work is less than this value.

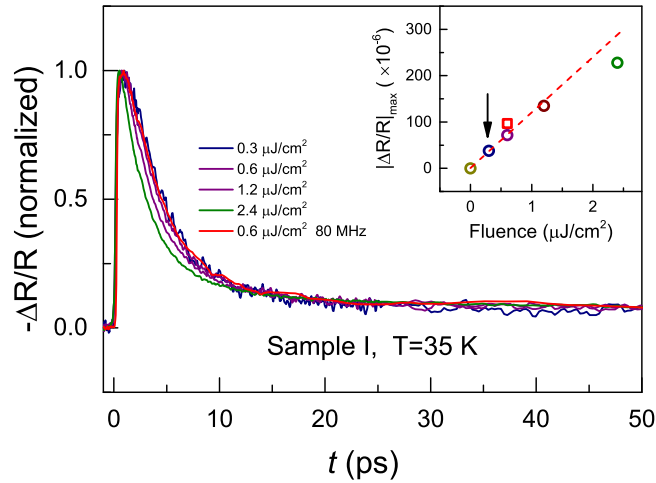


FIG. 4. Fluence-dependent  $\Delta R/R$  measurements for sample I ( $T_c = 18.6$  K) at 35 K using 5.1- and 80-MHz laser systems. The inset shows the maximum values of  $|\Delta R/R|$  as a function of fluence; the dashed line is a linear fit to the data (open circles). In the inset, the red open square corresponds to a pump fluence of  $\sim 0.6 \mu\text{J}/\text{cm}^2$  for the 80-MHz laser system. The black arrow indicates the fluence ( $\sim 0.3 \mu\text{J}/\text{cm}^2$ ) used in the main text.

#### APPENDIX B: EFFECTIVE-TEMPERATURE MODEL

The energy transfer rate between nonequilibrium charge carriers and phonons in the two-temperature model is connected to the Eliashberg coupling spectra function  $\alpha^2 F(\Omega)$  and was solved by Allen [43]. Very recently, a similar theoretical frame was extended to include  $I^2 \chi(\Omega)$ , associated with the bosonic excitations with electronic origin. The corresponding energy transfer rate is defined as [13,14]

$$G(\Pi_j, T_j, T_e) = \frac{6C_e}{\pi \hbar k_B^2 T_e} \int_0^\infty \Pi_j(\Omega) \Omega^2 [n(\Omega, T_j) - n(\Omega, T_e)] d\Omega, \quad (\text{B1})$$

where  $j$  ( $= s, p, l$ ) represents the electronic excitations ( $s$ ), hot phonons ( $p$ ), and the rest of the lattice ( $l$ );  $[\alpha^2 F(\Omega)]_{p,l}$  and  $I^2 \chi(\Omega)$  are represented by  $\Pi_{p,l}(\Omega)$  and  $\Pi_s(\Omega)$ , respectively. The total bosonic spectral function  $\Pi(\Omega)$  is defined as  $\Pi(\Omega) = \Pi_p(\Omega) + \Pi_l(\Omega) + \Pi_s(\Omega)$ .  $T_e$  is the electronic temperature, and  $T_j$  is the effective temperature characterizing each type of bosonic excitation.  $n(\Omega, T)$  is the Bose-Einstein distribution and is given by  $n(\Omega, T) = 1/(e^{\Omega/k_B T} - 1)$ . Here, the Fermi-Dirac distribution is assumed to build up instantaneously

after photoexcitation. Therefore, the energy transfer between nonequilibrium fermionic quasiparticles ( $T_e$ ) and bosonic excitations ( $T_j$ ), schematically shown in Fig. 2(a), can be described by the effective-temperature model via a set of coupled rate equations:

$$\frac{\partial T_e}{\partial t} = \frac{G(\Pi_s, T_s, T_e)}{C_e} + \frac{G(\Pi_p, T_p, T_e)}{C_e} + \frac{G(\Pi_l, T_l, T_e)}{C_e} + \frac{p(t)}{C_e}, \quad (\text{B2})$$

$$\frac{\partial T_s}{\partial t} = -\frac{G(\Pi_s, T_s, T_e)}{C_s}, \quad (\text{B3})$$

$$\frac{\partial T_p}{\partial t} = -\frac{G(\Pi_p, T_p, T_e)}{C_p} + \frac{g_{pl}}{C_p} (T_l - T_p), \quad (\text{B4})$$

$$\frac{\partial T_l}{\partial t} = -\frac{G(\Pi_l, T_l, T_e)}{C_l} - \frac{g_{pl}}{C_l} (T_l - T_p), \quad (\text{B5})$$

where  $p(t)$  is the Gaussian-like excitation source,  $C_e$  or  $C_j$  is the specific heat, and  $g_{pl}$  describes the coupling between hot phonons and the rest of the lattice due to the anharmonic decay process [44]. The  $g_{pl}$  coupling term is neglected in previous studies [14]. But our work shows that it has to be included for temperature-dependent experiments to fit the  $\Delta R/R$  data. The couplings between phonons and electronic excitations are ignored [14], mainly due to the instantaneous equilibration of  $T_e$  and  $T_s$ . In general, the specific heat of each subsystem satisfies the relation  $C_s < C_e < C_p \ll C_l$ . Additionally, the electron-phonon coupling function  $\Pi_{p,l}(\Omega)$  is expected to be temperature independent [34,36]. The detailed fitting procedure is given in the Supplemental Material [29].

When the nonthermal electrons have to be taken into account for the fitting, an extension of the above effective-temperature model can be used according to Ref. [33]. The essential part of the extended model is that on the right side of each above rate equation there will be an additional distinct heat source corresponding to the electrons or bosons. These terms are expressed as  $\partial U_{ee}/\partial t$ ,  $\partial U_{es}/\partial t$ ,  $\partial U_{ep}/\partial t$ , and  $\partial U_{el}/\partial t$ , respectively. They are given in detail in Ref. [33]. Compared with the effective-temperature model, the introduction of these terms will not add extra free fitting parameters for a given  $e-e$  scattering time  $\tau_{ee}$ . To check the potential contribution to  $C_s$  from the nonthermal electrons, we arbitrarily set several  $\tau_{ee}$  between 5 fs and 1 ps. In fact, a good fit can be obtained only for  $\tau_{ee}$  less than 100 fs.

- [1] B. Batlogg, R. Cava, A. Jayaraman, R. van Dover, G. Kourouklis, S. Sunshine, D. Murphy, L. Rupp, H. Chen, and A. White, Isotope Effect in the High- $T_c$  Superconductors  $\text{Ba}_2\text{YCu}_3\text{O}_7$  and  $\text{Ba}_2\text{EuCu}_3\text{O}_7$ , *Phys. Rev. Lett.* **58**, 2333 (1987).
- [2] M. Norman, H. Ding, J. Campuzano, T. Takeuchi, M. Randeria, T. Yokoya, T. Takahashi, T. Mochiku, and K. Kadowaki, Unusual Dispersion and Line Shape of the Superconducting State Spectra of  $\text{Bi}_2\text{Sr}_2\text{CaCu}_2\text{O}_{8+\delta}$ , *Phys. Rev. Lett.* **79**, 3506 (1997).

- [3] A. Damascelli, Z. Hussain, and Z.-X. Shen, Angle-resolved photoemission studies of the cuprate superconductors, *Rev. Mod. Phys.* **75**, 473 (2003).
- [4] E. H. da Silva Neto, R. Comin, F. He, R. Sutarto, Y. Jiang, R. L. Greene, G. A. Sawatzky, and A. Damascelli, Charge ordering in the electron-doped superconductor  $\text{Nd}_{2-x}\text{Ce}_x\text{CuO}_4$ , *Science* **347**, 282 (2015).
- [5] M. Le Tacon, A. Bosak, S. M. Souliou, G. Dellea, T. Loew, R. Heid, K.-P. Bohnen, G. Ghiringhelli, M. Krisch, and B. Keimer,

- Inelastic X-ray scattering in  $\text{YBa}_2\text{Cu}_3\text{O}_{6.6}$  reveals giant phonon anomalies and elastic central peak due to charge-density-wave formation, *Nat. Phys.* **10**, 52 (2014).
- [6] E. M. Motoyama, G. Yu, I. M. Vishik, O. P. Vajk, P. K. Mang, and M. Greven, Spin correlations in the electron-doped high-transition-temperature superconductor  $\text{Nd}_{2-x}\text{Ce}_x\text{CuO}_{4\pm\delta}$ , *Nature (London)* **445**, 186 (2007).
- [7] M. Fujita, M. Matsuda, S.-H. Lee, M. Nakagawa, and K. Yamada, Low-Energy Spin Fluctuations in the Ground States of Electron-Doped  $\text{Pr}_{1-x}\text{LaCe}_x\text{CuO}_{4\pm\delta}$  Cuprate Superconductors, *Phys. Rev. Lett.* **101**, 107003 (2008).
- [8] F. Niestemski, S. Kunwar, S. Zhou, S. Li, H. Ding, Z. Wang, P. Dai, and V. Madhavan, A distinct bosonic mode in an electron-doped high-transition-temperature superconductor, *Nature (London)* **450**, 1058 (2007).
- [9] E. Schachinger, C. C. Homes, R. P. S. M. Lobo, and J. P. Carbotte, Multiple bosonic mode coupling in the charge dynamics of the electron-doped superconductor  $(\text{Pr}_{2-x}\text{Ce}_x)\text{CuO}_4$ , *Phys. Rev. B* **78**, 134522 (2008).
- [10] Y. Onose, Y. Taguchi, K. Ishizaka, and Y. Tokura, Doping Dependence of Pseudogap and Related Charge Dynamics in  $\text{Nd}_{2-x}\text{Ce}_x\text{CuO}_4$ , *Phys. Rev. Lett.* **87**, 217001 (2001).
- [11] C. Giannetti, F. Cilento, S. Dal Conte, G. Coslovich, G. Ferrini, H. Molegraaf, M. Raichle, R. Liang, H. Eisaki, M. Greven, A. Damascelli, D. van der marel, and F. Parmigiani, Revealing the high-energy electronic excitations underlying the onset of high-temperature superconductivity in cuprates, *Nat. Commun.* **2**, 353 (2011).
- [12] H. Matsui, K. Terashima, T. Sato, T. Takahashi, S.-C. Wang, H.-B. Yang, H. Ding, T. Uefuji, and K. Yamada, Angle-Resolved Photoemission Spectroscopy of the Antiferromagnetic Superconductor  $\text{Nd}_{1.87}\text{Ce}_{0.13}\text{CuO}_4$ : Anisotropic Spin-Correlation Gap, Pseudogap, and the Induced Quasiparticle Mass Enhancement, *Phys. Rev. Lett.* **94**, 047005 (2005).
- [13] C. Giannetti, M. Capone, D. Fausti, M. Fabrizio, F. Parmigiani, and D. Mihailovic, Ultrafast optical spectroscopy of strongly correlated materials and high-temperature superconductors: A non-equilibrium approach, *Adv. Phys.* **65**, 58 (2016).
- [14] S. Dal Conte, C. Giannetti, G. Coslovich, F. Cilento, D. Bossini, T. Abebaw, F. Banfi, G. Ferrini, H. Eisaki, M. Greven, A. Damascelli, D. van der Marel, and F. Parmigiani, Disentangling the electronic and phononic glue in a high- $T_c$  superconductor, *Science* **335**, 1600 (2012).
- [15] J. Kogoj, M. Mierzejewski, and J. Bonca, Nature of Bosonic Excitations Revealed by High-Energy Charge Carriers, *Phys. Rev. Lett.* **117**, 227002 (2016).
- [16] J. Demsar, B. Podobnik, V. Kabanov, T. Wolf, and D. Mihailovic, Superconducting Gap  $\Delta_c$ , the Pseudogap  $\Delta_p$ , and Pair Fluctuations above  $T_c$  in Overdoped  $\text{Y}_{1-x}\text{Ca}_x\text{Ba}_2\text{Cu}_3\text{O}_{7-\delta}$  from Femtosecond Time-Domain Spectroscopy, *Phys. Rev. Lett.* **82**, 4918 (1999).
- [17] Y. H. Liu, Y. Toda, K. Shimatake, N. Momono, M. Oda, and M. Ido, Direct Observation of the Coexistence of the Pseudogap and Superconducting Quasiparticles in  $\text{Bi}_2\text{Sr}_2\text{CaCu}_2\text{O}_{8+y}$  by Time-Resolved Optical Spectroscopy, *Phys. Rev. Lett.* **101**, 137003 (2008).
- [18] E. E. M. Chia, J.-X. Zhu, D. Talbayev, R. D. Averitt, A. J. Taylor, K.-H. Oh, I.-S. Jo, and S.-I. Lee, Observation of Competing Order in a High- $T_c$  Superconductor using Femtosecond Optical Pulses, *Phys. Rev. Lett.* **99**, 147008 (2007).
- [19] P. Kusar, J. Demsar, D. Mihailovic, and S. Sugai, A systematic study of femtosecond quasiparticle relaxation processes in  $\text{La}_{2-x}\text{Sr}_x\text{CuO}_4$ , *Phys. Rev. B* **72**, 014544 (2005).
- [20] J. P. Hinton, J. D. Koralek, G. Yu, E. M. Motoyama, Y. Lu, A. Vishwanath, M. Greven, and J. Orenstein, Time-Resolved Optical Reflectivity of the Electron-Doped  $\text{Nd}_{2-x}\text{Ce}_x\text{CuO}_{4\pm\delta}$  Cuprate Superconductor: Evidence for an Interplay between Competing Orders, *Phys. Rev. Lett.* **110**, 217002 (2013).
- [21] I. M. Vishik, F. Mahmood, Z. Alpichshev, N. Gedik, J. Higgins, and R. L. Greene, Ultrafast dynamics in the presence of antiferromagnetic correlations in electron-doped cuprate  $\text{La}_{2-x}\text{Ce}_x\text{CuO}_{4\pm\delta}$ , *Phys. Rev. B* **95**, 115125 (2017).
- [22] G. Bianchi, C. Chen, M. Nohara, H. Takagi, and J. F. Ryan, Competing phases in the superconducting state of  $\text{La}_{2-x}\text{Sr}_x\text{CuO}_4$ : Temperature- and magnetic-field-dependent quasiparticle relaxation measurements, *Phys. Rev. B* **72**, 094516 (2005).
- [23] C. Gadermaier, A. S. Alexandrov, V. V. Kabanov, P. Kusar, T. Mertelj, X. Yao, C. Manzoni, D. Brida, G. Cerullo, and D. Mihailovic, Electron-Phonon Coupling in High-Temperature Cuprate Superconductors Determined from Electron Relaxation rates, *Phys. Rev. Lett.* **105**, 257001 (2010).
- [24] K. Jin, N. P. Butch, K. Kirshenbaum, J. Paglione, and R. L. Greene, Link between spin fluctuations and electron pairing in copper oxide superconductors, *Nature (London)* **476**, 73 (2011).
- [25] N. P. Armitage, P. Fournier, and R. L. Greene, Progress and perspectives on electron-doped cuprates, *Rev. Mod. Phys.* **82**, 2421 (2010).
- [26] H. Saadaoui, Z. Salman, H. Luetkens, T. Prokscha, A. Suter, W. A. MacFarlane, Y. Jiang, K. Jin, R. L. Greene, E. Morenzoni, and R. F. Kiefl, The phase diagram of electron-doped  $\text{La}_{2-x}\text{Ce}_x\text{CuO}_{4-\delta}$ , *Nat. Commun.* **6**, 6041 (2015).
- [27] J. Qi, T. Durakiewicz, S. A. Trugman, J.-X. Zhu, P. S. Riseborough, R. Baumbach, E. D. Bauer, K. Gofryk, J.-Q. Meng, J. J. Joyce, A. J. Taylor, and R. P. Prasankumar, Measurement of Two Low-Temperature Energy Gaps in the Electronic Structure of Antiferromagnetic  $\text{USb}_2$  Using Ultrafast Optical Spectroscopy, *Phys. Rev. Lett.* **111**, 057402 (2013).
- [28] M. C. Wang, S. Qiao, Z. Jiang, S. N. Luo, and J. Qi, Unraveling Photoinduced Spin Dynamics in the Topological Insulator  $\text{Bi}_2\text{Se}_3$ , *Phys. Rev. Lett.* **116**, 036601 (2016).
- [29] See Supplemental Material at <http://link.aps.org/supplemental/10.1103/PhysRevB.97.155157> for sample characterization and detailed fitting procedures, which includes Refs. [45–50].
- [30] V. V. Kabanov, J. Demsar, and D. Mihailovic, Kinetics of a Superconductor Excited with a Femtosecond Optical Pulse, *Phys. Rev. Lett.* **95**, 147002 (2005).
- [31] N. P. Butch, K. Jin, K. Kirshenbaum, R. L. Greene, and J. Paglione, Quantum critical scaling at the edge of Fermi liquid stability in a cuprate superconductor, *Proc. Natl. Acad. Sci. USA* **109**, 8440 (2012).
- [32] J. D. Rameau, S. Freutel, A. F. Kemper, M. A. Sentef, J. K. Freericks, I. Avigo, M. Ligges, L. Rettig, Y. Yoshida, H. Eisaki, J. Schneeloch, R. D. Zhong, Z. J. Xu, G. D. Gu, P. D. Johnson, and U. Bovensiepen, Energy dissipation from a correlated system driven out of equilibrium, *Nat. Commun.* **7**, 13761 (2016).
- [33] E. Carpene, Ultrafast laser irradiation of metals: Beyond the two-temperature model, *Phys. Rev. B* **74**, 024301 (2006).

- [34] F. Cilento, S. Dal Conte, G. Coslovich, F. Banfi, G. Ferrini, H. Eisaki, M. Greven, A. Damascelli, D. van der Marel, and F. Parmigiani, In search for the pairing glue in cuprates by non-equilibrium optical spectroscopy, *J. Phys.: Conf. Ser.* **449**, 012003 (2013).
- [35] J. Demsar, R. D. Averitt, K. H. Ahn, M. J. Graf, S. A. Trugman, V. V. Kabanov, J. L. Sarrao, and A. J. Taylor, Quasiparticle Relaxation Dynamics in Heavy Fermion Compounds, *Phys. Rev. Lett.* **91**, 027401 (2003).
- [36] F. Schmitt, W. S. Lee, D.-H. Lu, W. Meevasana, E. Motoyama, M. Greven, and Z.-X. Shen, Analysis of the spectral function of  $\text{Nd}_{1.85}\text{Ce}_{0.15}\text{CuO}_4$  obtained by angle-resolved photoemission spectroscopy, *Phys. Rev. B* **78**, 100505 (2008).
- [37] S. R. Park, D. J. Song, C. S. Leem, C. Kim, C. Kim, B. J. Kim, and H. Eisaki, Angle-Resolved Photoemission Spectroscopy of Electron-Doped Cuprate Superconductors: Isotropic Electron-Phonon Coupling, *Phys. Rev. Lett.* **101**, 117006 (2008).
- [38] K. Jin, X. Zhang, P. Bach, and R. L. Greene, Evidence for antiferromagnetic order in  $\text{La}_{2-x}\text{Ce}_x\text{CuO}_4$  from angular magnetoresistance measurements, *Phys. Rev. B* **80**, 012501 (2009).
- [39] P. B. Allen and R. Dynes, Transition temperature of strong-coupled superconductors reanalyzed, *Phys. Rev. B* **12**, 905 (1975).
- [40] A. J. Millis, S. Sachdev, and C. M. Varma, Inelastic scattering and pair breaking in anisotropic and isotropic superconductors, *Phys. Rev. B* **37**, 4975 (1988).
- [41] D. J. Scalapino, A common thread: The pairing interaction for unconventional superconductors, *Rev. Mod. Phys.* **84**, 1383 (2012).
- [42] H. J. Kang, P. Dai, J. W. Lynn, M. Matsuura, J. R. Thompson, S.-C. Zhang, D. N. Argyriou, Y. Onose, and Y. Tokura, Antiferromagnetic order as the competing ground state in electron-doped  $\text{Nd}_{1.85}\text{Ce}_{0.15}\text{CuO}_4$ , *Nature (London)* **423**, 522 (2003).
- [43] P. B. Allen, Theory of Thermal Relaxation of Electrons in Metals, *Phys. Rev. Lett.* **59**, 1460 (1987).
- [44] L. Perfetti, P. A. Loukakos, M. Lisowski, U. Bovensiepen, H. Eisaki, and M. Wolf, Ultrafast Electron Relaxation in Superconducting  $\text{Bi}_2\text{Sr}_2\text{CaCu}_2\text{O}_{8+\delta}$  by Time-Resolved Photoelectron Spectroscopy, *Phys. Rev. Lett.* **99**, 197001 (2007).
- [45] H. J. Kaufmann, E. G. Maksimov, and E. K. H. Salje, Electron-phonon interaction and optical spectra of metals, *J. Supercond.* **11**, 755 (1998).
- [46] S. G. Sharapov and J. P. Carbotte, Effects of energy dependence in the quasiparticle density of states on far-infrared absorption in the pseudogap state, *Phys. Rev. B* **72**, 134506 (2005).
- [47] J. Hwang, J. P. Carbotte, and T. Timusk, Evidence for a Pseudogap in Underdoped  $\text{Bi}_2\text{Sr}_2\text{CaCu}_2\text{O}_{8+\delta}$  and  $\text{YBa}_2\text{Cu}_3\text{O}_{6.50}$  from In-Plane Optical Conductivity Measurements, *Phys. Rev. Lett.* **100**, 177005 (2008).
- [48] H. Balci and R. L. Greene, Anomalous Change in the Field Dependence of the Electronic Specific Heat of an Electron-Doped Cuprate Superconductor, *Phys. Rev. Lett.* **93**, 067001 (2004).
- [49] A. Iwai, M. Abe, H. Nakajima, and K. I. Kumagai, Heat capacity of the electron-doped  $\text{Pr}_{2-x}\text{Ce}_x\text{CuO}_4$ , *Phys. C (Amsterdam, Neth.)* **185-189**, 1349 (1991).
- [50] P. Richard, M. Neupane, Y.-M. Xu, P. Fournier, S. Li, P. Dai, Z. Wang, and H. Ding, Competition between Antiferromagnetism and Superconductivity in the Electron-Doped Cuprates Triggered by Oxygen Reduction, *Phys. Rev. Lett.* **99**, 157002 (2007).